Dalton Transactions

ROYAL SOCIETY OF CHEMISTRY

FRONTIER

View Article Online
View Journal | View Issue

Cite this: *Dalton Trans.*, 2026, **55**, 4387

Cooperative E–H bond insertions and activations by transition metal complexes (E = B, C, Si, and Al): hemilability at play

Suvam Saha, Stutee Mohapatra and Sundargopal Ghosh *

The cooperative activation and insertion of E–H σ-bonds at transition metal centers represent a powerful strategy for synthetic chemistry and catalysis (E = B, C, Si, Al). In recent years, hemilabile ligand frameworks capable of dynamically switching between coordinated and dissociated states have emerged as key enablers of such reactivity. Their ability to modulate electronic and steric environments around the metal center promotes synergistic metal–ligand cooperation (MLC). This Frontier article highlights recent advances in E–H bond activation and insertion processes typically mediated by transition metal complexes bearing hemilabile donor sites, with particular emphasis on mechanistic insights, bonding features, and the design principles governing ligand flexibility. Also, particular attention is given to σ-borane and σ-borate intermediates and C–H and Si–H bond cleavage. The emerging understanding of reversible coordination, metal–ligand bond polarity and ligand-assisted proton/hydride shuttling highlight hemilability as a central tool in developing next-generation catalytic platforms for sustainable synthesis and energy-relevant transformations.

Received 27th December 2025,
Accepted 17th February 2026

DOI: 10.1039/d5dt03092g

rsc.li/dalton

Introduction

Transition metal complexes play a pivotal role in the activation of bonds such as C–H, B–H, and Si–H, thereby advancing the broad field of homogeneous catalysis.[1] Typically, such activations take place at the metal center through elementary processes such as oxidative addition, reductive elimination, and β-hydride elimination (Chart 1a). Although ligands bound to the metal help stabilize the complex and modulate its reactivity patterns through electronic and steric effects, they generally do not play an active role in the primary bond activation event. Interestingly, over the past few decades, extensive studies have focused on the cooperative involvement of both the metal and the ligand in E–H (E = H, C, B, Si, Al, and Sn) bond activation, a concept widely recognised as metal–ligand cooperation (MLC) (Chart 1a).[2] Systems that involve MLC in the rudimentary steps of catalytic processes have provided greater efficiency in both reactivity and selectivity terms as compared to the conventional approaches. Nature offers precedents for this concept, particu-

Department of Chemistry, Indian Institute of Technology Madras, Chennai, India. E-mail: sghosh@iitm.ac.in

Suvam Saha

Suvam Saha received his B.Sc. in Chemistry from Ramakrishna Mission Residential College, Narendrapur, India, in 2016. Then, he obtained M.Sc. in Chemistry from IIT Madras, India, in 2018. He is currently a Ph.D. student at IIT Madras. His research area focuses mostly on small-molecule activation through metal–ligand cooperativity.

Stutee Mohapatra

Stutee Mohapatra received her B. Sc. degree in Chemistry from Dhenkanal Autonomous College, Odisha, in 2018, followed by an M.Sc. degree from the Central University of Tamil Nadu in 2020. She is currently pursuing her Ph.D. at IIT Madras, where her research focuses on groups 6 and 8 metallaborane chemistry.

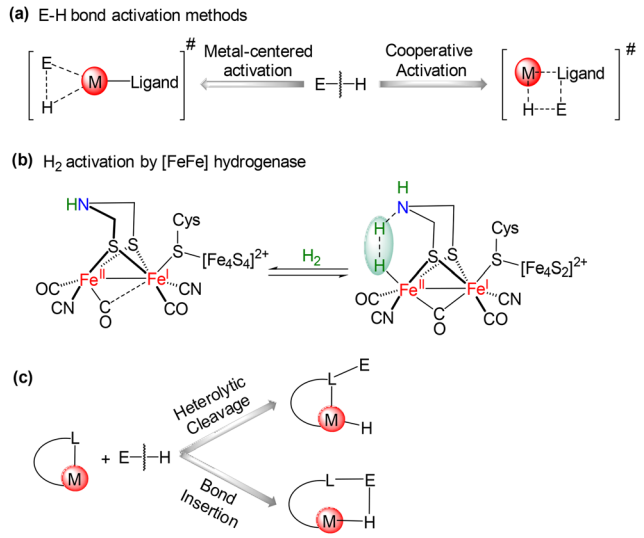

Chart 1 (a) Methods for E–H bond activation; (b) inspiration from nature for MLC; (c) modes of MLC involving hemilabile ligands.

larly in enzymatic catalysis such as dehydrogenation by [FeFe] and [FeNi] hydrogenases.[3] Fujiwara's pioneering study on palladium acetate-mediated C–H activation laid the foundation for the MLC concept in homogeneous catalysis.[4]

Subsequently, the extensive application of this strategy in cooperative H_2 activation paved the way for its extension to other small molecules such as boranes, silanes, and alumanes.[2,5]

In MLC systems, ligands can act as Lewis bases and Lewis acids or undergo aromatisation/de-aromatisation to facilitate E–H bond activation.[6] Also, redox non-innocent ligands can serve as electron reservoirs to regulate the metal oxidation state throughout the process. Thus, the ligand design is the most crucial aspect of the MLC approach for the E–H bond activation. In general, ligands can coordinate to metals through one or multiple binding sites, engaging in L-, X-, or Z-type interactions as classified by the covalent bond classification (CBC) system proposed by Green and Parkin.[7] Due to the chelate effect, polydentate ligands offer increased stability and a higher degree of coordination environment of a metal in catalysis compared to monodentate ligands. While any heterobidentate ligand features a hard and a soft donor site, it can create vacant sites at the metal center readily under catalytic conditions and can be classified as a hemilabile ligand. Thus, based on the hard–soft acid–base (HSAB) principle developed by Pearson,[8] the reactivity of hemilabile ligand coordinated metal complexes can be postulated. For instance, group 3–4 transition metals of higher oxidation states as well as lanthanides can be considered hard sites and they preferentially bind to the harder donor site of a heterobidentate hemilabile ligand. This results in weakening of the softer donor site-metal bond and eventually it becomes more susceptible to E–H bond activation. In contrast, softer late transition metal complexes with hemilabile ligands tend to activate E–H bonds through the harder donor site. Therefore, the careful selection of metal and ligand is an essential requirement for MLC.

Among the hemilabile bidentate ligands, the MLC activation of E–H bonds by 1,3-coordinated and 1,4-coordinated transition metal complexes has been studied extensively.[9] These ligand frameworks are likewise widespread in nature, where they play key roles in processes such as proton transfer and element–hydrogen bond activation, among others. The purpose of this Frontier article is to survey the influence of hemilabile heterobidentate ligands on early and late transition metal centers, with emphasis on their 1,3- and 1,4-chelation modes in facilitating E–H bond activation (E = B, C, Si) *via* MLC. The E–H bond activations dictated by the HSAB principle in such complexes and their catalytic applications will be discussed. Simultaneously, the E–H bond insertions into the metal–ligand bonds or the MLC bonding of boranes or silanes, generating several unique molecules which are very interesting in terms of exploring novel bonding motifs and their utilization in catalysis will be presented. The scope of this Frontier article is summarised in Chart 2.

B–H bond activation by MLC

Boranes are important in synthesis and are being explored as carbon-free energy carriers, driving strong interest in B–H bond activation.[1e] While oxidative addition to transition

Sundargopal Ghosh

Sundargopal Ghosh is a professor at the Indian Institute of Technology Madras, India. His primary research focuses on the synthesis of polyhedral metallaborane clusters, transition metal diboranes and Bn (n = 3–6) ring systems, as well as transition metal borane/borate complexes for small-molecule activation.

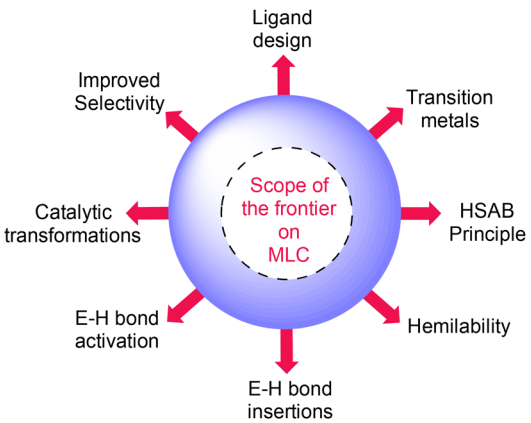

Chart 2 Scope of this Frontier article.

metals remains a key strategy, metal–ligand cooperativity (MLC) has recently emerged as a powerful alternative, enabling efficient B–H activation and insertion processes that support catalytic formation of organoboron and other valuable products.[1,2] Cooperative B–H binding has also uncovered unique bonding motifs in low-boron transition-metal complexes, such as boryl, borylene, σ-borate, and diborane species.[1b,10] This Frontier article highlights recent advances in MLC-enabled B–H activation using ligand hemilability, focusing on ligand effects and resulting catalytic applications.

Early transition metals

In 2020, Wang *et al.* reported a half-sandwich molybdenum thiolate complex [Cp*Mo(1,2-$Ph_2PC_6H_4S$)(η^2-NCMe)] (**1**), which contains a Mo–P–C–C–S five membered ring and a η^2-MeCN ligand (Scheme 1).[11] Complex **1** was found to be an efficient catalyst for the transfer hydrogenation of nitriles using [BH_3·NH_3] at room temperature. To gain mechanistic insight into this transformation, complex **1** was treated with [BH_3·NH_3] under ambient conditions. An immediate colour change from yellow to brown was observed, and the reaction afforded the Mo(II) hydride complex **2**. Single-crystal X-ray diffraction analysis of **2** confirmed heterolytic B–H bond cleavage *via* Mo–S cooperation. Complex **2** features both a terminal Mo–H hydride and a bridging Mo–H–B hydride, forming a well-defined four-membered Mo–S–B–H metallacycle. The ^{11}B NMR resonance at δ = −24.2 ppm is consistent with a borane-like ligand environment. The ^{1}H NMR spectrum of **2** displayed three sets of hydride signals at δ = −4.49, −4.65, and −7.15 ppm as broad peaks, which were assigned to Mo–H–B–H, Mo–H–B–H and Mo–H, respectively. Notably, in the presence of ammonia, complex **2** mediates the reduction of nitriles to the corresponding amines. The combined mechanistic experiments and computational studies indicate that, during nitrile reduction with [BH_3·NH_3], the NH_3 moiety serves as the source of the amine N–H hydrogens, whereas the BH_3 fragment provides the methylene (CH_2) hydrogens incorporated into the final amine product. These observations support a mechanism in which cooperative B–H bond activation is the key elementary step.

The donor atoms in the 2-phosphinothiolate ligand of **1** are predominantly soft in nature. Probably, the lone pair on sulfur plays a decisive role in stabilising the BH_2 unit formed upon the heterolytic cleavage of the B–H bond. Motivated by these observations, we sought to investigate the reactivity of Mo(II) complexes supported by bidentate chelating ligands that feature a combination of both soft and hard donor sites. To synthesise such a complex, the salt elimination reaction between [Cp*Mo(CO)$_3$Me] and [K(2-mercaptobenzothiazolyl)] was carried out, which afforded the complex [Cp*Mo(CO)$_2${κ^2-*N,S*-($NC_7H_4S_2$)}] (**3a**) (Scheme 2).[12a] In **3a**, the soft Mo(II) center is chelated by the 2-mercaptobenzothiazolyl ligand through a soft S and a harder N donor, generating a strained four-membered Mo–N–C–S metallacycle. The reactivity of **3a** with [BH_3·THF] was examined; however, this resulted in decomposition of **3a**. In contrast, using a different method, we have synthesised a W analogue of **3a**, [Cp*W(CO)$_2${κ^2-N,S-($NC_7H_4S_2$)}] (**3b**), from the photolytic treatment of [Cp*W(CO)$_3$Me] with borate salts.[12b] The reaction of **3a** and **b** with bulkier boranes $MesBH_2$ and 3,5-trifluoromethylbenzene borane led cleanly to the formation of [Cp*M(CO)$_2${κ^2-*S,H*-(NBH_2R)($NC_7H_4S_2$)}] (**4a**: M = Mo, R = Mes; **4b**: M = Mo, R = Ar^F, and **4c**: M = W, R = Ar^F) (Scheme 2).[12] The crystal structure of **4a** displays a nonplanar six-membered molybdenacycle (MoHBNCS) generated from a hemilabile ring opening of the Mo–N bond followed by the capture of H_2BMes. Considering sulfur as a soft base, it binds more strongly to soft Mo(II) centers as compared to hard N. Therefore, the insertion of borane occurs *via* cleavage of the weaker Mo–N bond in **3a**. There is an elongation of approximately 15% in the Mo–coordinated B–H bond relative to the corresponding free B–H bond, consistent with significant activation and partial weakening of the B–H linkage upon coordination to the Mo(II) centre. The ^{11}B NMR resonance for **4a** at δ = −15.5 ppm is consistent with a borane-like ligand environment. However, computational studies suggest a bonding situation with mixed borane/borate character. The reaction of **3b** with a bulky borane yielded an analogous σ-borate complex of

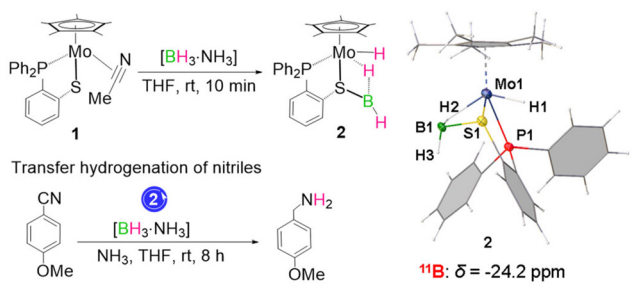

Scheme 1 B–H bond activation by a 1,4-P,S-chelated molybdenum complex. Reproduced from ref. 11 with permission from American Chemical Society,[11] copyright 2020.

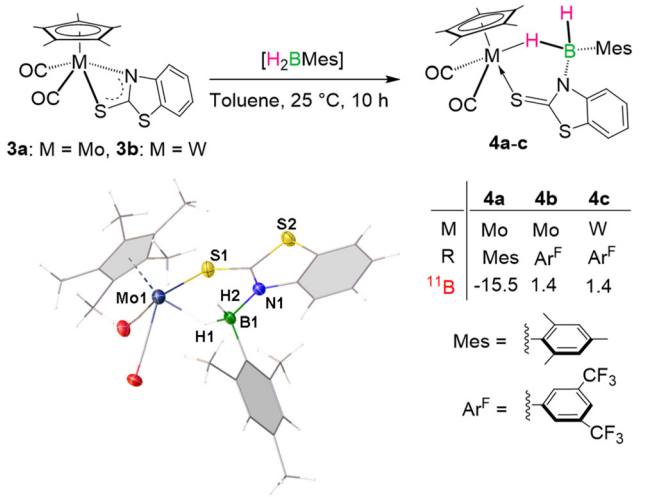

Scheme 2 B–H bond activation by a 1,3-N,S-chelated molybdenum complex.[12]

tungsten, **4c**. Due to the electron-poor boron center in **4b** and **4c**, the ^{11}B chemical shifts are more deshielded than that of **4a**.

Leitner and co-workers have synthesised a Mn P–N–P pincer complex, $[Mn(Ph_2PCH_2SiMe_2)_2NH(CO)_2Br]$ (**5**) (Scheme 3), *via* a salt elimination reaction between $[Mn(CO)_5Br]$ and the 1,3-bis ((diphenyl-phosphino)methyl)tetramethyldi-silazane ligand.[13] Complex **5** proved to be an excellent catalyst for the challenging reduction of C=O units of carboxylic acids, carbonic acid derivatives and even CO_2, utilising pinacolborane as a reducing agent. The mechanistic investigation showed that complex **5** converts to **5a** containing a Mn=N bond in the presence of a base. The addition of pinacolborane to **5a** led to the formation of a manganese σ-borate complex **6**, which contains a four-membered Mn–H–B–N ring. Complex **6** converts slowly to a Mn–H complex, evident from NMR experiments. These observations suggest a complete heterolytic cleavage of the B–H bond by metal–ligand cooperation.

Late transition metals

Oestreich and co-workers reported the synthesis of a coordinatively unsaturated ruthenium complex, $[(DmpS)Ru(PR_3)][BAr^F_4]$ (Dmp = 2,6-dimesitylphenyl), **7**, characterized by a strongly polarized Ru–S interaction (Scheme 4).[14] When the reactivity of **7** toward a range of substituted boranes was examined using NMR techniques, the resulting saturated adducts, **8**, exhibited upfield B–H signals, as compared to the uncoordinated boranes. Structural analysis of one of these adducts revealed an unusual arrangement in which boron binds to the sulfur donor while the corresponding hydrogen bridges to the Ru center, forming a four-membered H–Ru–B–S ring system. In this species, the B–H bond is significantly elongated (1.55 Å), approximately 30% longer than in a typical B–H bond, consistent with substantial activation. The complex can be interpreted

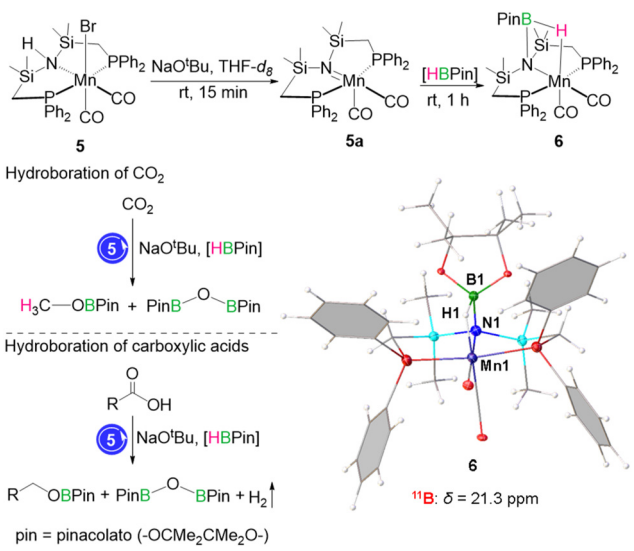

Scheme 3 B–H bond activation by a Mn–N bond.[14]

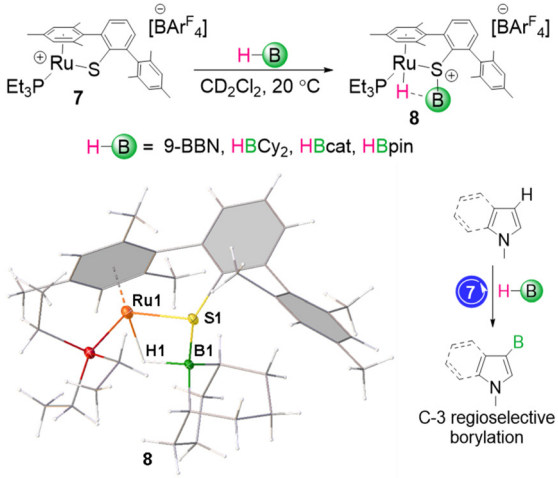

Scheme 4 B–H bond activation and borenium cation formation by a ruthenium–thiolate complex. Reproduced from ref. 14 with permission from American Chemical Society,[14] copyright 2013.

as the product of σ-bond metathesis at the B–H unit, generating a ruthenium hydride in combination with a sulfur-stabilized borenium fragment. The same system was subsequently utilized as a catalyst for the dehydrogenative borylation of indoles and pyrroles, where the proposed reaction pathway involves initial electrophilic borylation at the heteroaromatic ring followed by deprotonation to yield the borylated products.

Several examples have been reported demonstrating the participation of metal carbene complexes in cooperative B–H bond activation.[15,16] In this context, Gessner and co-workers reported the B–H bond activation of several boranes using the Ru–carbene complex **9** (Scheme 5).[16b] Upon reaction with cate-

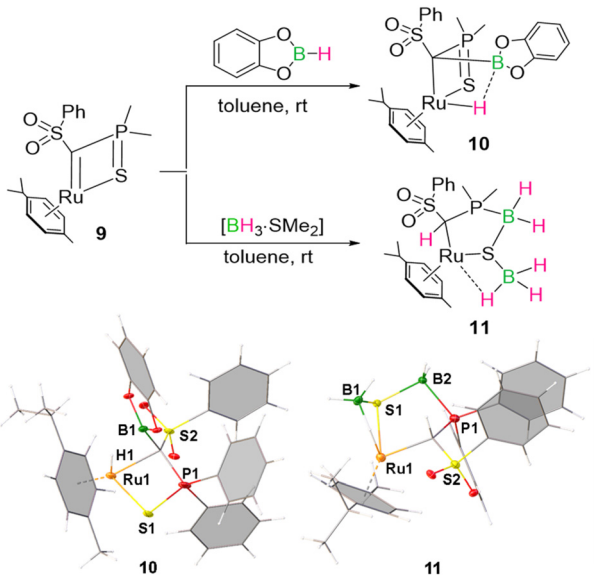

Scheme 5 B–H bond activation by a ruthenium–carbene complex. Reproduced from ref. 16b with permission from John Wiley and Sons,[16b] copyright 2018.

cholborane, complex **9** underwent B–H bond cleavage across the Ru=C bond to afford complex **10**. The molecular structure of **10** revealed a slightly pyramidalized boron center, with a sum of angles of 351.0°, indicating an interaction between the boron atom and the Ru–H bond, as further supported by natural bond orbital (NBO) analysis. Although the B···H distance (1.68 Å) in **10** is longer than that of a typical B–H bond, as well as those involved in agostic interactions with a metal center, it is consistent with a weak secondary interaction. Interestingly, treatment of **9** with [BH_3·SMe_2] led to the activation of two borane units, yielding complex **11**. One B–H bond of a BH_3 molecule was activated *via* coordination at the Ru–S bond, whereas a B–H bond of a second BH_3 unit was fully cleaved, resulting in protonation of the carbene carbon atom and insertion of a BH_2 moiety into the P–S bond of **9**. Complex **11** can be described either as a ruthenium hydride bearing a boryl-substituted thioether ligand or as a thiolato complex featuring BH_3 coordination along the Ru–S linkage. Notably, the reactivity of **9** toward pinacolborane was found to be similar to that observed with [BH_3·SMe_2].

In 2009, the Stradiotto group synthesised a coordinatively unsaturated ruthenium complex, [Cp*Ru(κ^2-P,O-L)] (L = 1-diisopropylphosphino-2-indanone), and utilised it in activation of various E–H bonds (E = H, B, and Si).[17] Similarly, while exploring the role of hemilabile 1,3-N,S-chelating ligands in metal–ligand cooperative (MLC) transformations, we serendipitously isolated a rare Ru(III) complex, [PR_3\{κ^2-N,S-($C_7H_4NS_2$)\}$_2$Ru\{κ^1-S-($C_7H_4NS_2$)\}] (**12**), featuring two κ^2-1,3-N,S-chelated rings, one pendant mercaptobenzothiazole unit, and a phosphine ligand (Scheme 6).[18] Remarkably, treatment of complex **12** with [BH_3·THF] afforded a bis-(σ-borate) species, [PPh_3Ru\{κ^3-H,S,S-(NH_2BSBH_2N)($S_2C_7H_4$)$_2$\}] (**13**), whereas the reaction with the bulky $MesBH_2$ yielded two unusual bis-(dihydroborate) complexes, [\{κ^3-S,H,H-(NH_2BMes)Ru($S_2C_7H_4$)\}$_2$] (*trans*-**14** and *cis*-**14**). In both transformations, dual-site borane insertion occurred across the two Ru–N bonds, accompanied by dissociation of the PPh_3 ligand. The formation of the B_2S core in **13** likely involves cleavage of the C–S bond of the dangling ligand in **12**, releasing benzothiazole. On the other hand, complete dissociation of the 2-mercaptobenzothiazolyl ligand leads to the generation of isomers of complex **14**. Notably, the ^{11}B NMR resonance of **13** (δ = −10.1 ppm) is significantly more shielded than those of *trans*-**14** (δ = 39.4 ppm) and *cis*-**14** (δ = 31.2 ppm), indicating a higher σ-donation of B–H bond to the metal in **13**.

We have also synthesised bis-1,3-*N,S*-chelated Ru(II) and Os(II) complexes **15a** and **b**, each containing two strained four-membered M–N–C–S metallacycles (Scheme 7).[19] Upon reaction with [BH_3·SMe_2], both complexes undergo B–H bond activation across the polar M–N bonds, albeit leading to different products. In the case of the Ru complex (**15a**), the borane unit inserts into the polar Ru–N bond to afford a ruthenium σ-borate complex (**16**) that retains a four-membered Ru–N–C–S ring framework (Scheme 7).[19b] In contrast, the Os(II) analogue (**15b**) promotes heterolytic B–H bond cleavage upon reaction with [BH_3·SMe_2], resulting in the formation of an osmium(σ-borate) hydride complex (**17**).[19c] The reaction is proposed to proceed *via* initial B–H bond cleavage across one Os–N bond to generate an osmium hydride intermediate, followed by clea-

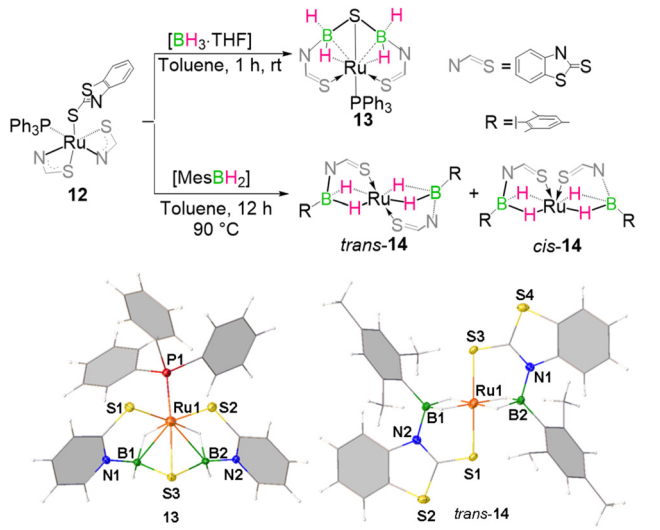

Scheme 6 Dual site B–H bond activation by a 1,3-N,S-chelated ruthenium(III) complex.[18]

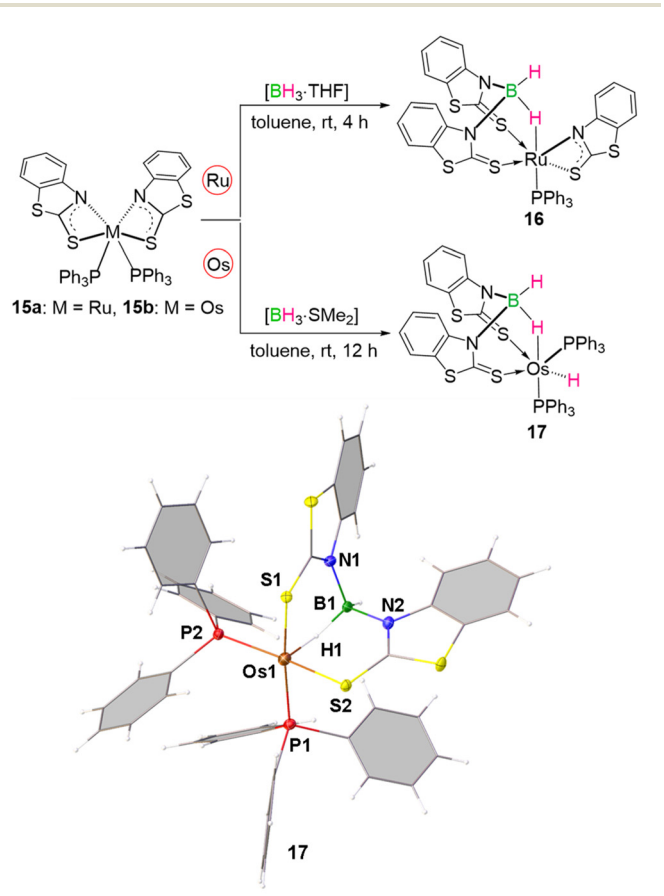

Scheme 7 B–H bond activations by bis-1,3-N,S-chelated ruthenium(II) and osmium(II) complexes.[19]

vage of the second Os–N bond to form a B–N bond. Subsequent coordination of one of the remaining B–H bonds of the $[BH_2L_2]$ fragment (L = 2-mercaptobenzothiazolyl) to the osmium center forms complex **17**. Although the Os–H hydride in **17** could not be observed in the solid-state X-ray diffraction analysis, its presence was confirmed by a sharp resonance at δ = −13.26 ppm in the ^{1}H NMR spectrum, which remained unchanged upon ^{11}B decoupling.

In contrast, the reaction of an analogous bis-κ^2-N,S-chelated iron(II) complex, $[(dppe)Fe\{\kappa^2\text{-}N,S\text{-}(mp)\}_2]$ (mp = 2-mercaptopyridyl) (**18**), with $[BH_3{\cdot}SMe_2]$ afforded a rare dimeric iron bis(dihydridoborate) complex, $[Fe\{\kappa^3\text{-}S,H,H\text{-}(H_2BH(mp))\}_2]_2$, ΛΔ/ΔΛ-**19**, isolated as a pair of enantiomers (Scheme 8).[20] Each enantiomer features an almost planar Fe1–S1–Fe2–S2 square core, with a C_2 axis of symmetry passing through the centre of this plane. The NMR studies reveal the formation of a monomeric bis-(dihydroborate) intermediate, $[Fe\{\kappa^3\text{-}S,H,H\text{-}(H_2BH(C_5H_4NS))\}_2]$, which subsequently undergoes dimerization to furnish ΛΔ/ΔΛ-**19**. These findings clearly illustrate that subtle variations in metal identity and ligand environment can steer the same MLC-assisted B–H insertion pathway toward distinct structural outcomes, enabling access to novel architectures.

Daly *et al.* reported the synthesis of a Ru(II) complex **20** supported by a triaryl, redox-active S_2N_2 ligand constructed from *o*-phenylenediamine and thioanisole fragments (Scheme 9).[21] Upon treatment of **20** with the reducing agent $[NaBH_4]$, the reaction afforded complex **21**, featuring dual metal–ligand cooperative coordination of two BH_3 units across the Ru–N bonds. Structural analysis revealed a notable elongation of the N–C bonds and a shortening of the NC–NC bonds in **21** relative to **20**, consistent with the reduction of the diiminoquinone framework to the corresponding *o*-phenylenediamine form. The ^{11}B NMR spectrum of **21** displayed a single resonance at δ = −9.3 ppm, while ^{1}H NMR measurements suggested the presence of three stereoisomers, attributable to different spatial orientations of the two SMe_2 substituents. In complexes **3a** and **b**, **12**, and **18**, the polarity of the M–N bonds governs B–H activation, whereas the metal–ligand cooperative binding of BH_3 in **21** is driven primarily by the reduction of the non-innocent ligand backbone, enabling coordination without cleavage of the M–N bonds.

A similar metal–ligand cooperative binding of BH_3 by a rigid tetradentate bisphosphine–bisamide $[PNNP]^{2-}$ ligand chelated Fe(II) complex (**22**) was reported by Thomas and coworkers (Scheme 10).[22] Dual-MLC bound BH_3 complex **23** shows a more shielded ^{11}B chemical shift at δ = −17.1 ppm than complex **21**. The ^{1}H chemical shifts for the M–H–B protons for **23** (δ = −15.40 ppm) are more shielded than those of **21** (δ = −9.56, −9.35 and −8.96 ppm for three stereoisomers), indicating more metal hydride character. The molecular structures of both **21** and **23** show the B–H binding generated two M–N–B–H metallacycles with an elongation of the B–H bonds (1.334 Å (**23**), 1.310 Å (**21**)) coordinated to metal atoms compared to the terminal B–H hydrogens (1.104 Å (**23**), 1.112 Å (**21**)), indicating cooperative B–H bond activation. The structural assessment and NMR spectroscopic data support the assignment of fully cleaved B–H bonds with weak Lewis acid/base interactions between the metal hydrides and borane fragments. A few other examples of MLC binding of boranes (**24–26**) have also been reported (Chart 3).[23]

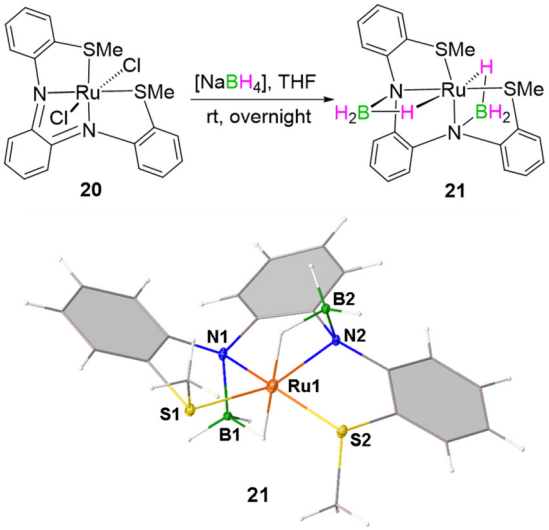

Scheme 9 B–H bond activation by a Ru–N bond. Reproduced from ref. 21 with permission from American Chemical Society,[21] copyright 2020.

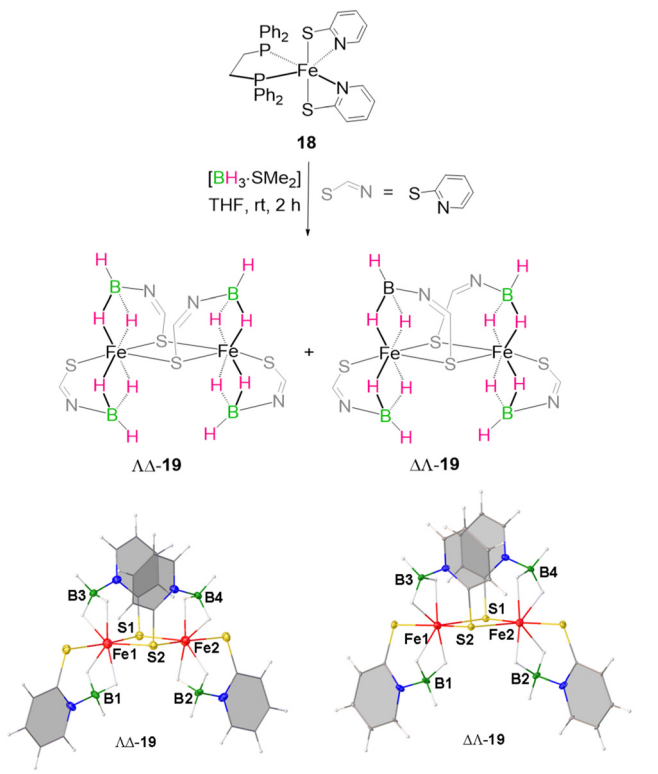

Scheme 8 Dual site B–H bond activation by a 1,3-N,S-chelated iron complex and dimerization of the dihydroborate complex.[20]

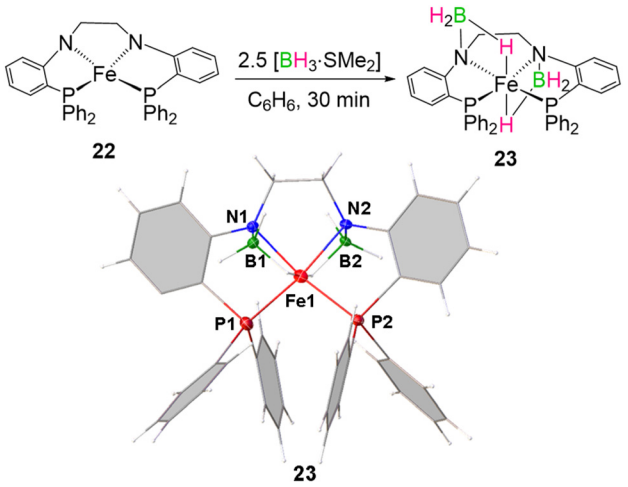

Scheme 10 B–H bond activation by an Fe–N bond. Reproduced from ref. 22 with permission from Royal Society of Chemistry,[22] copyright 2020.

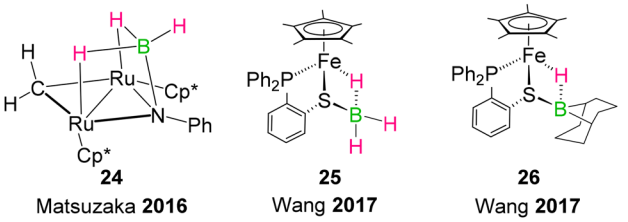

Chart 3 Examples of MLC binding of BH_3.[23]

Schafer and Love *et al.* synthesised 1,3-N,O-chelated Rh and Ir complexes [M{κ²-*N,O*-Xyl(N)P(O)(OEt)$_2$}(η⁴-cod)] (**27a**: Rh, **27b**: Ir) containing a M–O–P–N four-membered ring. The harder O-center and a relatively softer N donor are coordinated to the soft Rh/Ir metals (Scheme 11), forming a hemilabile framework. Upon treatment with bulky cyclohexylborane ($HBCy_2$), the borane is captured by the M–O bonds of **27a** and **b** generating six-membered M–N–P–O–B–H metallacycles in **28a** and **b**.[24] The ^{11}B chemical shifts for **28a** and **b** (δ = 13.0 ppm (**28a**) and δ = 14.6 ppm (**28b**)) are substantially shielded compared to those of free Cy_2BH (δ = 59.0 ppm), consistent with Shimoi-type O → B bonding along with B–H σ-donation to the metal center. The B–H bond distances (1.310 Å (**28a**), 1.41 Å (**28b**)) are considerably longer than the free B–H bond distances, indicating B–H bond activation (Scheme 11).

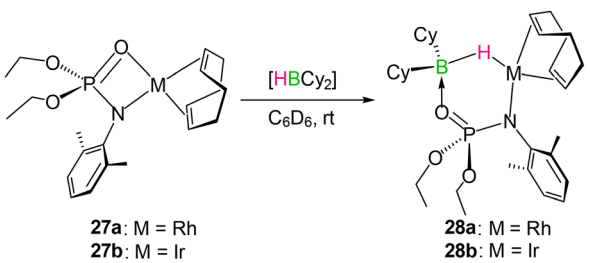

Scheme 11 B–H bond insertion by 1,3-N,O-chelated Rh/Ir complexes.[24]

Complexes **28a** and **b** promote chemoselective hydroboration of aldehydes even in the presence of an alkyne (Scheme 12). When free $HBCy_2$ or the Lewis base-stabilised borane complex [$(EtO)_3P{\cdot}BHCy_3$] is used, alkyne hydroboration proceeds, as observed with 1-octyne.[24] In contrast, the use of complexes **28b** results in inverse chemoselectivity, where aldehyde hydroboration dominates. The change in selectivity cannot be attributed solely to Lewis-base stabilization of the borane, thereby indicating a substantial role of MLC. The proposed mechanism for hydroboration involves activation through either M–H–B bond cleavage or P═O–B bond cleavage, enabling capture of the small molecule and generating boron-functionalized products. The hydroboration regenerates the initial complexes **27a** and **b**, thereby closing the catalytic cycle.

Recently, a series of κ²-N,L-chelated Ir and Rh complexes, [Cp*M(κ¹-*E*-C_5H_4NL)(κ²-N,L-C_5H_4NX)], (**29a**: M = Ir, L = S; **29b**: M = Ir, L = Se; **29c**: M = Rh, L = S; and **29d**: M = Rh, L = Se) were synthesised by us through salt-metathesis reactions of [$CpMCl_2$]$_2$ with the corresponding thio- or seleno-pyridyl potassium salts (Scheme 13).[25] These complexes feature one ligand bound in a κ¹-L mode, while the second adopts a κ²-N,L chelation pattern, generating strained four-membered metallacycles with unusually small bite angles (≈68°). Exposure of the Ir derivatives (**29a** and **b**) to [$BH_3{\cdot}THF$] produces two distinct classes of products: monometallic diborane(5) complexes, [(Cp*Ir^{III}H){κ³-*B,B,L*-(B_2H_4-C_5H_4NL)}] (**30a**: E = S, **30b**: E = Se),

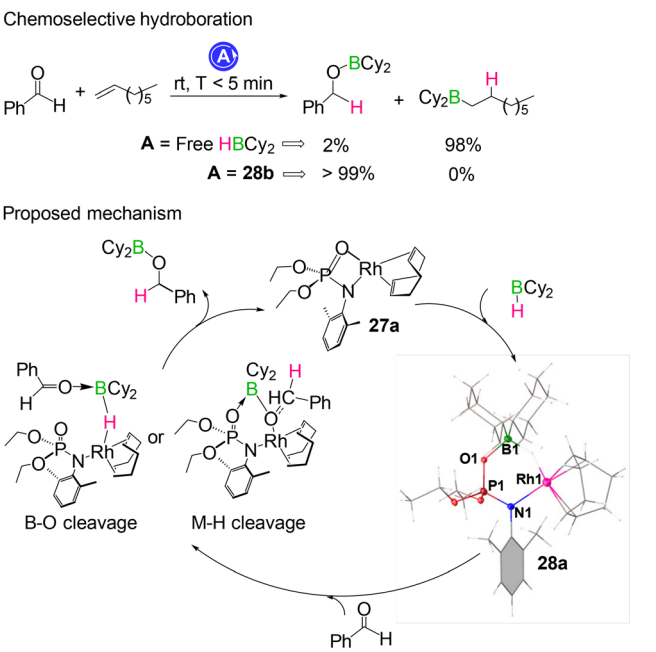

Scheme 12 Chemoselective hydroboration of aldehydes *via* MLC. Reproduced from ref. 24 with permission from John Wiley and Sons,[24] copyright 2016.

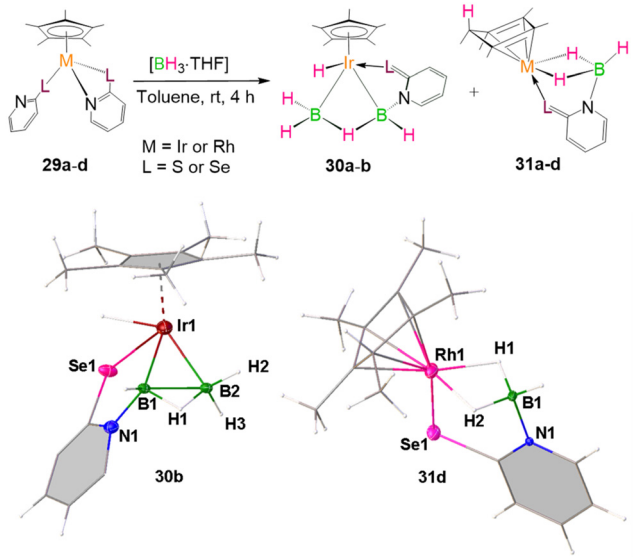

Scheme 13 B–H bond activation by MLC and dehydrogenative B–B homocoupling.[25]

and Ir(I) dihydroborate complexes, [(η^4-C_5Me_5H)Ir^I{κ^2-*H,H,L*-(H_3B-C_5H_4NL)}] (**31a:** L = S, **31b:** L = Se).[21] The diborane(5) species **30a** and **b** stabilize a rare non-classical $[B_2H_4(C_5H_4NL)]^-$ fragment, plausibly formed through MLC-assisted B–H activation at the Ir–N site followed by dehydrogenative B–B coupling. We have earlier synthesised a bimetallic template based classical diborane(5) complex and a monometallic classical diborane(6) complex, in which the formation involves no ligand cooperation.[26] In contrast, the Rh analogues (**29c** and **d**) undergo B–H insertion into the Rh–N bond to yield Rh(I) dihydroborate complexes, [(η^4-C_5Me_5H)Rh^I{κ^3-*H,H,L*-(H_3B-C_5H_4NL)}] (**31c:** L = S, **31d:** L = Se), accompanied by Cp* ring slippage. These divergent outcomes highlight the distinct reactivity profiles of Ir and Rh toward B–H activation within strained κ^2-N,L ligand environments.

Moving to Group 10 metals, Wang and co-workers synthesised half-sandwich Ni(II) complexes of the type [Cp*Ni(1,2-$R_2PC_6H_4X$)] (**32a:** X = O, R = Ph; **32b:** X = NH, R = Ph), featuring M–P–C–C–O/N five-membered metallacycles (Scheme 14).[27] Complexes **32a** and **b** readily undergo heterolytic cleavage of the B–H bond in HBPin to form the corresponding nickel hydride complexes **33a** and **b**. Interestingly, B–H activation by the Ni–O complex **32a** is reversible, whereas the Ni–N analogue **32b** mediates irreversible activation. As a consequence, in the catalytic hydroboration of N-heterocycles, the Ni–O system **32a** exhibits significantly superior performance compared to the Ni–N complex **32b**.[27]

Recently Gunanathan *et al.* synthesised a stable pyridine based Cu(II) NNN pincer complex, **34**, which utilizes ammonia borane as a hydrogen source to facilitate the 1,2-reduction of quinolines (Scheme 15).[28] Based on the several experimental studies, they have proposed a plausible mechanism for this catalytic process. Complex **34** undergoes dehydrohalogenation in the presence of a base to form an amide complex, **35**, which

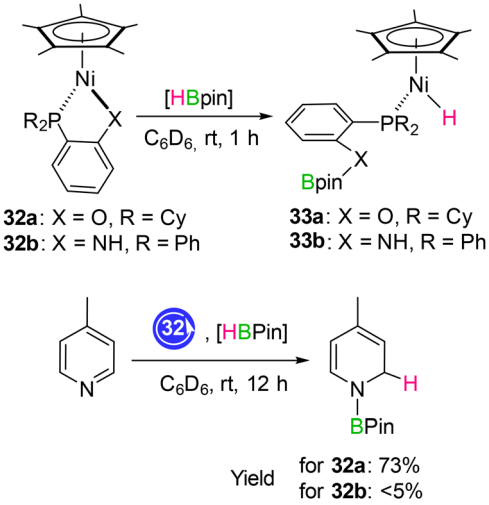

Scheme 14 B–H bond activation at Ni–N and Ni–O bonds.[27]

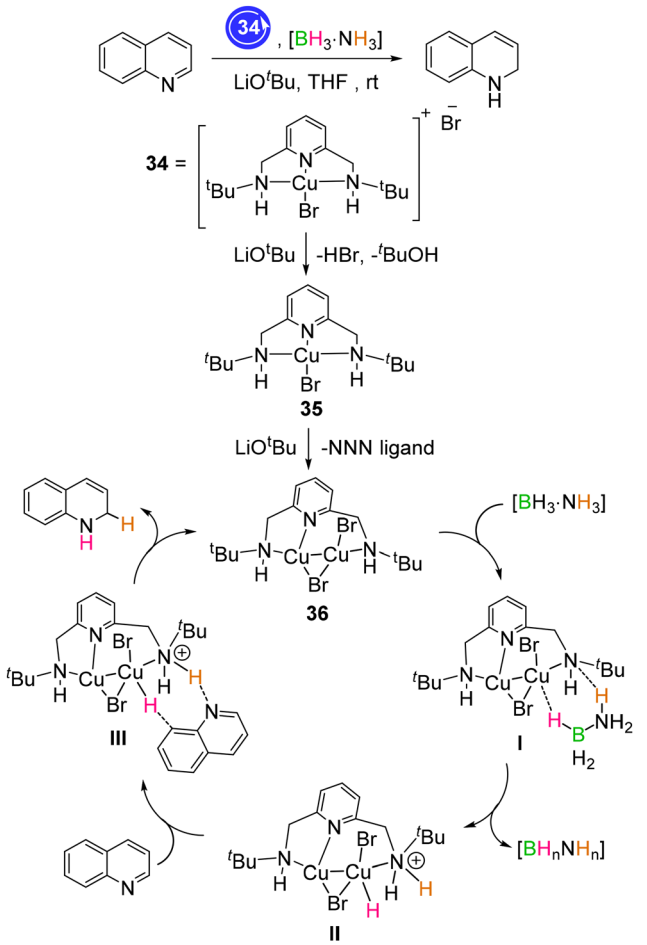

Scheme 15 B–H bond activation and utilization as a hydride source.[28]

further undergoes disproportionation to yield an active catalyst **36**. Complex **36** may have coordinated with $[NH_3{\cdot}BH_3]$ to form the intermediate **I**. This intermediate possibly transfers

hydrides to the metal and ligand center simultaneously to form **II** by releasing borazine. Eventually, intermediate **II** may have been reduced with quinoline selectively to form 1,2-dihydroquinoline and regenerate the catalytically active species **36**. The metal–ligand cooperative activation of B–H and N–H bonds is crucial for the catalytic transformation.

Si–H bond activation by MLC

Metal-mediated and metal–ligand cooperative (MLC) Si–H bond activation processes have been studied extensively, owing to the relatively low bond dissociation energy of the Si–H bond, which is comparatively lower than that of H–H. This reduced bond strength renders the Si–H activation as an attractive pathway for accessing value-added organosilicon compounds. Although significant progress has been made, examples of Si–H bond activation *via* metal–ligand cooperation remain relatively uncommon. One of the earliest examples of MLC-driven Si–H activation was reported by Tilley and coworkers, who showed that a Ta=N bond in tantalum imido complexes can heterolytically cleave Si–H bonds (Chart 4).[29] Subsequent studies by Andersen, Clot, and others revealed analogous reactivity at Ti=N and Ti=S bonds.[30] In this Frontier article, recent advances in Si–H bond cleavage, insertion processes, and their emerging catalytic applications will be highlighted.

As discussed earlier, based on the dual site B–H bond activation across the Fe–N (amide) linkage of the 18-electron low-spin bis(amido)bis(phosphine) Fe(II) complex **22**, Thomas *et al.* have utilised it for the activation of the Si–H bonds of primary silanes (Scheme 16).[31] Treatment of complex **22** with two equivalents of $PhSiH_3$ affords the Fe–Hydride complex **43** *via* Si–H bond activation followed by dehydrogenation. The molecular structure of **43** reveals that two Si–H bonds have been cleaved across Fe–N linkages by two independent units of **22** (Scheme 16). In the resulting complex, the Si–H bonds are elongated by at least 10% relative to those in free silanes. The absence of significant $^{1}J_{Si-H}$ coupling for the Fe-hydride signals (H1 and H2) indicates minimal M–H···Si interaction and supports a predominantly Fe–H character, consistent with typical Fe–H bond lengths. In contrast, H3 lies farther from the Fe centers. Computational analysis shows that H1 and H2 function as Fe hydrides involved in **3c–2e** Fe–H–Si interactions,

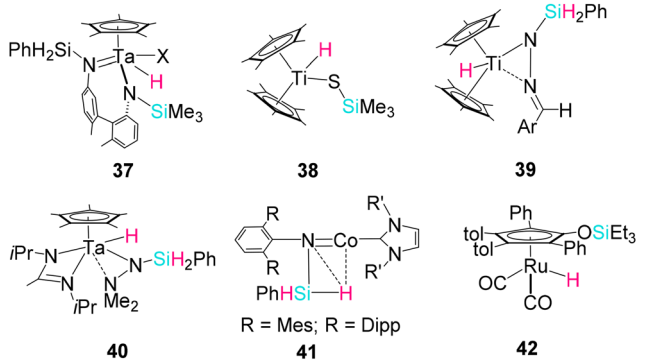

Chart 4 Si–H activations by M–N or M–S bonds.[29,30]

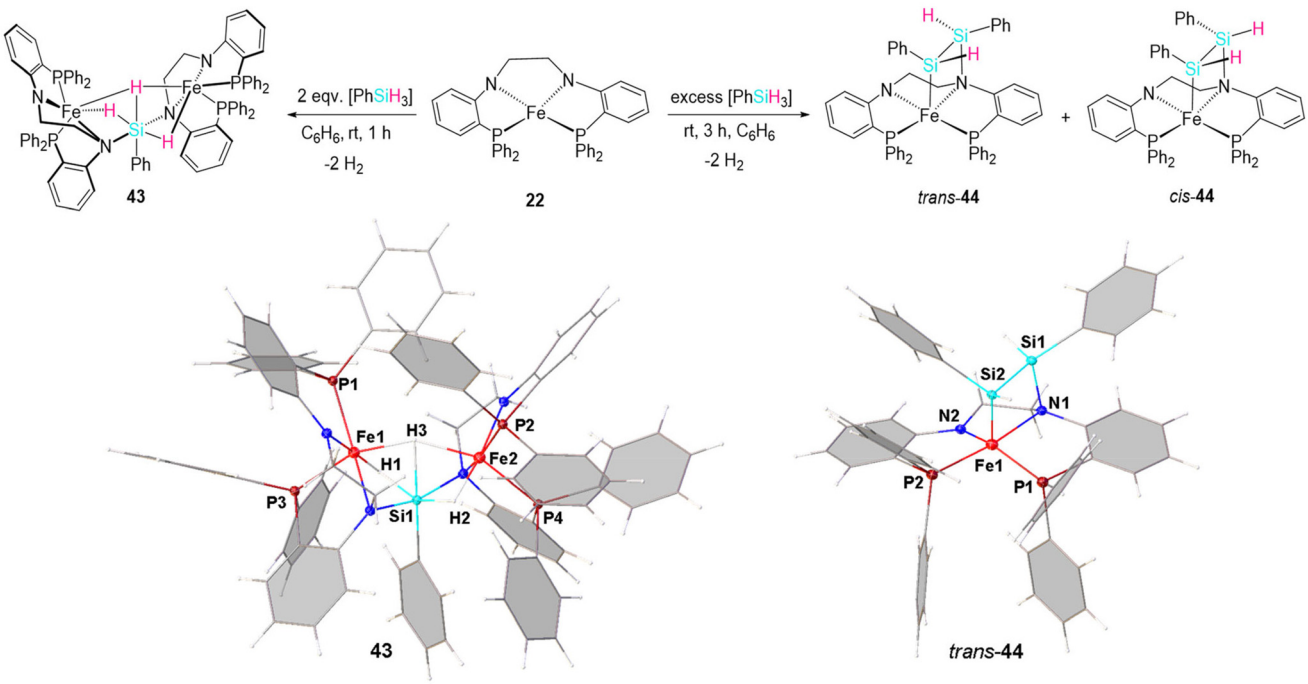

Scheme 16 Si–H activation and silane coupling across an Fe–amide bond. Reproduced from ref. 31 with permission from American Chemical Society,[31] copyright 2023.

whereas Si–H3 behaves as a Si hydride engaged in a weaker, agostic-type **4c–2e** interaction with the Fe centers. Interestingly, when excess silane was reacted with **22**, it led to the isolation of a mixture of two *trans* and *cis* isomers of iron silyl complex **44** in a 3 : 2 ratio (Scheme 16). The solid-state structure of one of the isomers, *trans*-**44**, revealed that two equivalents of $PhSiH_3$ have undergone dehydrogenative coupling across the Fe–amide linkage to form a new Si–Si bond, accompanied by the release of two equivalents of H_2. The Si–Si (2.307 Å) bond distance in *trans*-**44** is also between those of a typical Si–Si and a Si=Si bond. Traditionally, Si–Si bond formation has relied on Wurtz-type coupling of halosilanes using alkali metals; however, these reactions often require harsh conditions and generate undesirable by-products. This was the first example of a Si–Si bond formation *via* MLC binding of Si–H bonds under ambient conditions.

Rauchfuss and co-workers have described the synthesis of an iron(II) diphosphine–dialkoxide dicarbonyl complex [Fe(LP_2O_2)$(CO)_2$] (**45**; P_2O_2 = $(Ph_2PC_6H_4CHO)_2^{2-}$) by the coupling of 2 equiv. of 2-diphenylphosphinobenzaldehyde in the presence of [Fe$(CO)_3$bda] (bda = benzylideneacetone) (Scheme 17).[32] Although complex **45** was unreactive towards H_2, it takes part in heterolytic Si–H bond activation of Ph_2SiH_2 to produce an Fe hydride complex [HFe[P_2O(OSiHPh_2)]$(CO)_2$] (**46**), bearing an *O*-silylated phosphine–alkoxide arm (Scheme 17). The hemilability of the ligand backbone plays a crucial part in this case. IR and NMR spectroscopic data support the presence of an Fe–H unit alongside silylation localized at oxygen, confirming ligand-centered Si–H engagement rather than further reaction at the metal. X-ray structural analysis verified the *endo* orientation of the siloxy substituent, demonstrating retention of stereochemistry at the ligand backbone. Notably, the complex remains stable even in excess Ph_2SiH_2, as the second alkoxide group does not undergo silylation, and the Si–H bond within the silylated product is unreactive toward another equivalent of the starting Fe-complex, reflecting steric shielding and electronic saturation at the remaining alkoxide.

In the course of our recent efforts for B–H bond activation, we have isolated several κ^2-*N,S*-chelated group 8 metal complexes. One of these complexes, **16** was thermolysed with 1.2 equiv. of Ph_2SiH_2 that led to the Si–H bond activation by the polar Ru–N bond yielding isomeric silyl complexes **47** and **47′** along with a trisilyl ruthenium hydride complex **48** in low yields (Scheme 18).[33] At higher temperature, the yield of **48** increases. The upfield ^{1}H chemical shift at δ = −10.56 ppm supports the presence of a Ru–H moiety. The ^{29}Si{^{1}H} NMR spectrum features a single resonance at δ = 55.8 ppm, which is in agreement with a symmetrical environment in **48**. The solid-state X-ray structure of **48** clearly confirms that the ruthenium center is coordinated to three silyl groups in an octahedral fashion together with a capped hydride ligand (Ru–H) (Fig. 1).

Moret *et al.* have reported the synthesis of multiple Ni(0) complexes **49a** and **b**, supported by a pincer-type ligand platform containing an imine moiety bridged by two/one *o*-phenylene linkers with phosphine substituents (PCNP). Reaction of the Ni PCNP complex **49a** with diphenylsilane in benzene yielded a single isolable product **50a**, arising from formal C=N hydrosilylation (Scheme 19).[34] N-SiPh_2H remains Ni-bound *via* η^2-Si–H σ-coordination, supported by ^{31}P NMR

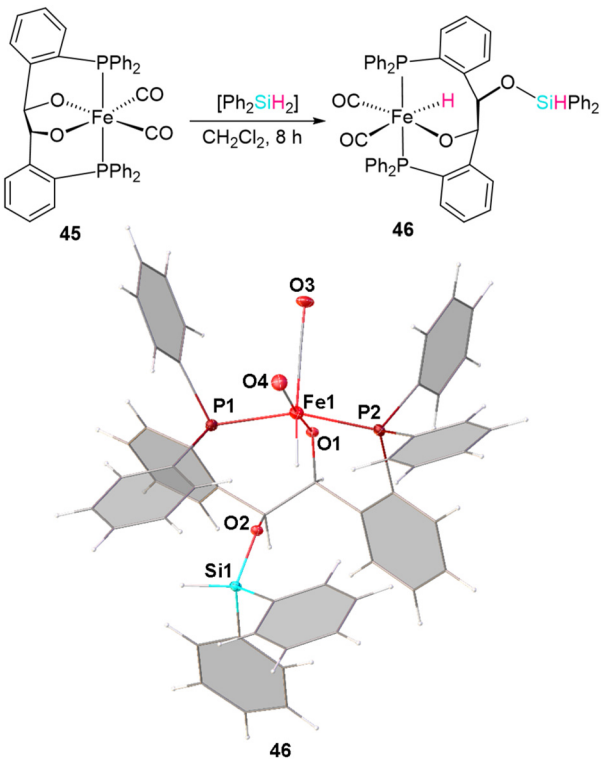

Scheme 17 Heterolytic Si–H cleavage across an Fe–O bond. Reproduced from ref. 32 with permission from American Chemical Society,[32] copyright 2015.

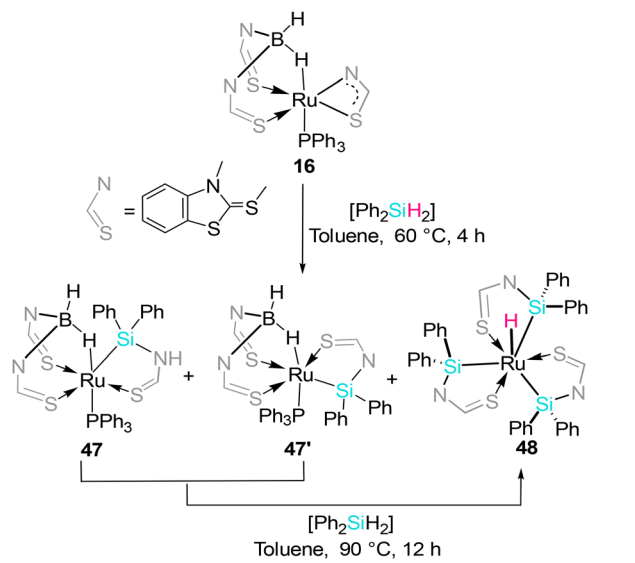

Scheme 18 Si–H bond activation by a κ^2-N,S-chelated ruthenium complex.[33]

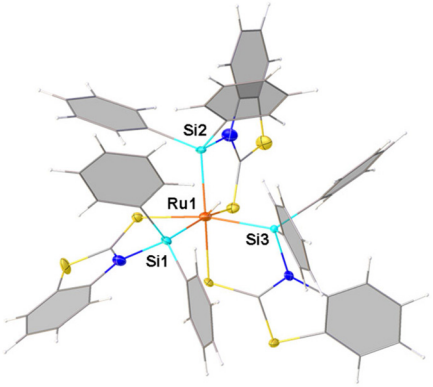

Fig. 1 Molecular structure of **48**.[33]

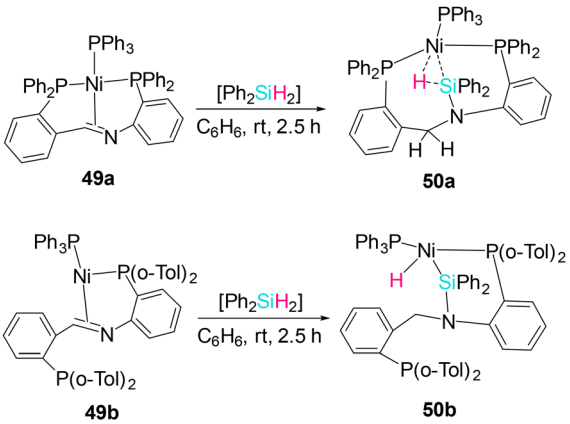

Scheme 19 Si–H activation by Ni-(PCNP)ligand cooperation.

(32.8, 17.1, 7.8 ppm, mutually coupled) and a hydridic ^{1}H at −2.77 ppm showing $^2J_{(H-Si)}$ = 109 Hz, consistent with η^2-Si–H binding rather than oxidative addition. To probe steric effects, *o*-tolyl Ni(0) complex **50b** was treated with diphenylsilane in C_6D_6, heterolytic cleavage of Si–H occurred yielding **50b**. DFT calculations suggest a cooperative Ni-mediated ligand-to-ligand hydrogen transfer as a key step. Interestingly, the degree of activation of the remaining Si–H bond in the product was found to strongly depend on the coordination number at Ni. Three-coordinate complex **50a** is best described as an η^2(Si,H) σ-complex. However, in **50b**, the Si–H bond is activated to a larger extent, and it is better viewed as a Ni(II) center bearing a silyl and a hydride ligand engaging in a secondary interaction.

Al–H bond activation by MLC

Coordination and activation of Al–H bonds exclusively at metal centres is well established. Nikonov and co-workers demonstrated the reversible oxidative addition of an Al–H bond to an Al(I) centre.[35] Subsequently, the Aldridge group reported σ(Al–H) coordination to group 6 transition metal centers in both κ^1 and κ^2 binding modes. In contrast, coordination of a β-diketiminato-supported alane to a cobalt centre resulted in an unusually high degree of Al–H bond activation.[36] Crimmin and colleagues described the coordination of hydroalumane to group 8 metals, leading to complexes that feature three-centre-two-electron (**3c–2e**) M–H–Al bonding motifs.[37] In fact, the aluminium based ligand supported transition metal complexes have been utilised in a variety of small molecule activations.[38,39] Despite these advances, examples of Al–H bond activation proceeding through metal–ligand cooperation are rare.

One notable example was reported by Oestreich and co-workers, who investigated the reaction of complex **7** with DIBAL-H, which rapidly afforded the hydroalane adduct **51** (Scheme 20).[5] In this complex, aluminium binds to the sulfur donor of the ligand framework, while the hydride is connected to the ruthenium centre. In a true sense, the hydroalane adduct (**51**) cannot be considered as a sulfur-stabilised aluminium ion.[40] The Al–H bond in **51** is significantly elongated relative to that in free hydroalanes, consistent with heterolytic Al–H bond cleavage. However, computational studies suggest that the bonding in **51** is better described as a σ(Ru–H) → Al donor–acceptor interaction. In addition to the Ru–H and Al–S linkages, a weak Ru···Al interaction is also evident. Importantly, the Ru–S-activated DIBAL-H adduct **51** was shown to promote C(sp^3)–F bond cleavage, and complex **7** proved to be a highly effective catalyst for hydrodefluorinative Friedel–Crafts alkylation of CF_3-substituted arenes, delivering unsymmetrical diarylmethanes with a broad range of arene nucleophiles.

C–H bond activation by MLC

C–H bond cleavage is one of the most important elementary reactions for several organic transformations. The chemistry of C–H activation has evolved significantly over the last 60 years, mainly utilizing sigma bond metathesis or concerted metalation deprotonation processes. The examples of metal–ligand cooperative C–H bond activation have emerged over the last decade. Ligand aromatization–dearomatization and metal–carbene bond mediated C–H bond activations are the most well known. However, the examples of hemilabile ligand participation in MLC C–H activation are quite limited and mostly the recent advances in the activation of C–H bonds of terminal alkynes will be discussed in this Frontier article. Notably, unlike the hydridic E–H (E = B, Al, and Si) bonds discussed above, the C–H bond of terminal alkynes is protic in nature.

The 1,3-*N*,*O*-chelated phosphoramidate complex, [Ir{κ^2-*N*,*O*-Xyl(N)P(O)(OEt)$_2$}(η^4-COD)] (**52**), was employed for C–H activation to utilize cooperation between Ir(III) and a hemilabile

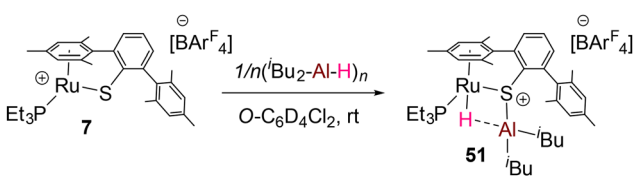

Scheme 20 Al–H bond activation by a polar Ru–S bond.[5]

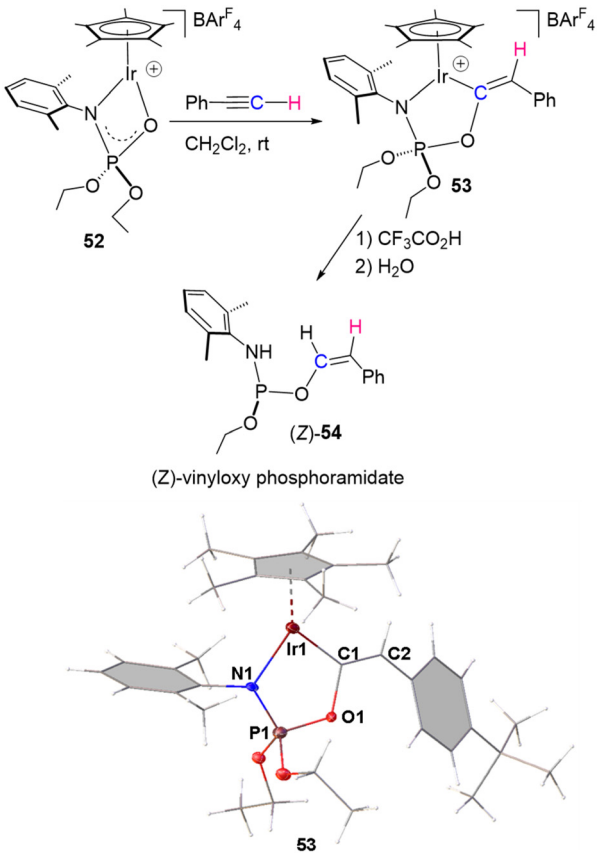

Scheme 21 Ligand-assisted proton shuttling by a 1,3-N,O-chelated phosphoramidate complex, **52**. Reproduced from ref. 41 with permission from American Chemical Society,[41] copyright 2016.

phosphoramidate ligand to develop a new chemical transformation: 1-alkyne *O*-phosphoramidation (Scheme 21).[41] The goal was to overcome the preference of alkyne functionalization reactions for Markovnikov or *N*-functionalized products, thereby enabling the synthetically important anti-Markovnikov *O*-functionalization pathway. Achieving such selectivity provides access to vinyl organophosphates, compounds of notable biological and synthetic importance. The reaction of **52** with a terminal alkyne results in a change from a four- to a five-membered metallacycle to give the 16-electron (*E*)-vinyloxy iridium (III) complex, $[Cp^*Ir(\kappa^2\text{-}N,C\text{-}(E)\text{-Xyl(N)P(O–C=C(H)(Ph))}(OEt)_2)]^+$ (**53**). Interestingly, under the mild acidic work-up conditions, complex **53** led to the isolation of (*Z*)-vinyloxy phosphoramidate **54** and a known aggregate $[Cp^*Ir(O_2CCF_3)_2(H_2O)]_n$. The hemilabile N,O-chelate plays an active role in the catalytic cycle, functioning as a proton shuttle (LAPS: ligand-assisted proton shuttle) and enabling reversible $[(O_2CCF_3)_2(H_2O)]_n$. coordination dynamics that facilitate alkyne activation and promote selective C–O bond formation at the terminal carbon. In accordance with the HSAB principle, the alkyne insertion occurred through the cleavage of the relatively weaker bond between the soft Ir and hard O compared to the softer N. This study nicely illustrated how ligand design and cooperative reactivity can be harnessed to override intrinsic regioselectivity in alkyne functionalization.

Maseras and Sola groups have demonstrated the effect of a hemilabile acetate ligand in C–H bond activation by MLC as compared to the transition metal based activation. The five coordinate Ru hydride complex $[Ru(Cl)H(CO)(P^iPr_3)_2]$ can react with 1 equivalent of phenylacetylene to produce a phenylacetylide derivative.[42a] However, when a 6-coordinate derivative [Ru(κ^2-acetate)H(CO)(P^iPr_3)$_2$] (**55**) reacts with phenylacetylene, it doesn't stop at the alkenyl derivative (**56**) (Scheme 22).[42b] In fact, complex **56** reacts with one more equivalent of phenylacetylene to produce complex **57** with the release of styrene. Computational studies revealed that this pathway is assisted by one oxygen atom of the hemilabile acetate ligand. This is followed by proton transfer to the alkenyl ligand, again mediated by the same acetate –OH functionality through a ligand-assisted proton shuttle (LAPS) mechanism. This cooperative sequence ultimately leads to styrene formation and the alkynyl complex **57**.

The hydroborate complexes of Ru, $[(k^2\text{-}N,S\text{-L})PR_3Ru\{\kappa^3\text{-}H,S,S'\text{-}H_2B(L)_2\}]$ (**16**) (R = Ph or Cy; L = $C_7H_4NS_2$) containing a strained four membered Ru–N–C–S ring synthesised by us have been proven to show hemilabile characteristics for small molecule activation. When they are employed for the C(sp)–H bond activation of terminal alkynes containing electron-withdrawing groups, it leads to the insertion of the alkynes into the Ru–N as well as Ru–S bonds to form complexes **58** and **59** (R′ = CO_2Me or $C_6H_4NO_2$), respectively (Scheme 23).[19a] At room temperature or under photolytic or mild thermolytic conditions, complex **58** is the major product. Interestingly, at higher temperatures, complex **58** was converted to **59**. This indicates that amination was favoured under milder conditions, while under harsher conditions thionation was more facile. Both complexes contain a five-membered ruthenacycle featuring an exocyclic C=C bond. Guided by earlier reports on LAPS-type processes, we proposed that the alkyne first undergoes metal-mediated activation, followed by proton transfer from the alkyne to the basic N,S-benzothiazolyl fragment. This is then succeeded by an intramolecular anti-Markovnikov attack by either the nitrogen or sulfur atom of the benzothiazo-

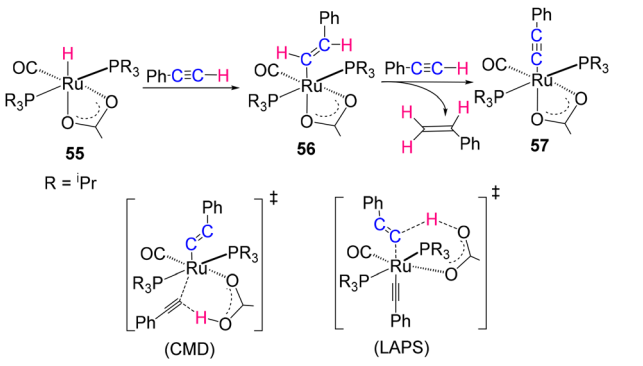

Scheme 22 Acetate assisted C–H bond activation and proton shuttle.[42b]

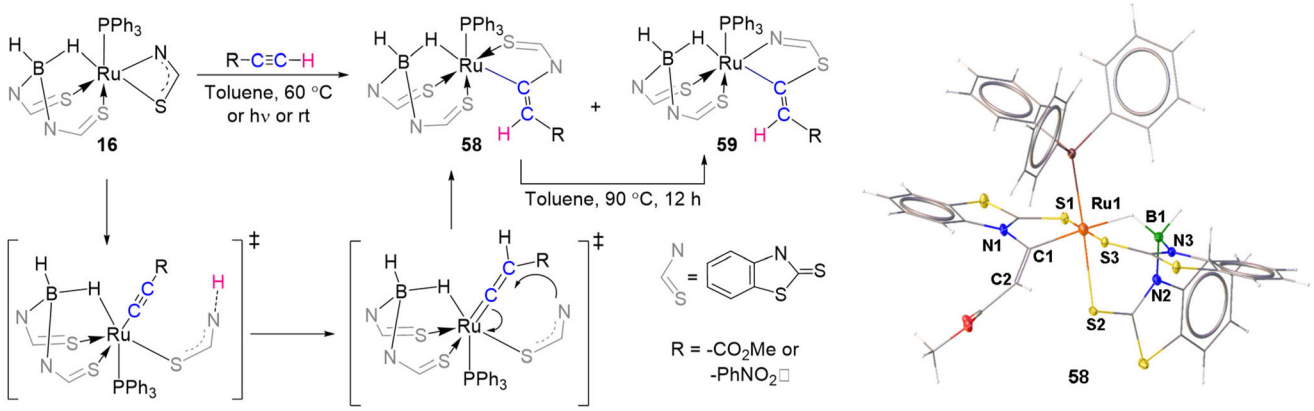

Scheme 23 Amination *vs.* thionation of alkynes by 1,3-N,S-chelated Ru–borate complexes.[19a]

lyl unit onto the activated alkyne. Overall, the reactions are consistent with a ligand-assisted proton shuttle (LAPS) mechanism, in which the nucleophilic N or S site of the benzothiazolyl group in **16** serves as an internal base, facilitating both the C–H activation step and subsequent bond-forming events.

In 2018, Albéniz and coworkers showed that the arylation of pyridines proceeds *via* a ligand-assisted C–H bond activation process. They employed 6-hydroxy-2,2′-bipyridyl (**L^1**) which is tautomeric with its ketone form, as a ligand to accomplish the efficient conversion of pyridine and 4-methyliodobenzene to 3-tolylpyridine successfully with good yield (Scheme 24).[43] However, when the 4-hydroxy-2,2′-bipyridyl (**L^2**) was utilised, the reaction didn't show satisfactory results. The theoretical studies show that the ligand-assisted concentrated deprotonation of pyridionate oxygen is a key step in the catalytic cycle. Therefore, the position of the keto group in the coordinating ligand in **60** is in the closest proximity to the Pd center, which facilitates C–H activation and subsequent palladation to form intermediate **61**. The catalytic process operates *via* a Pd(0)/Pd (II) redox cycle. Notably, cleavage of the *meta*-C–H bond is energetically favoured, consistent with the observed regioselectivity in the product distribution.

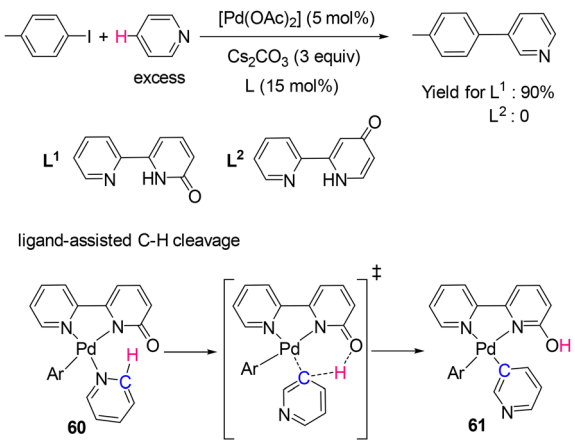

Scheme 24 Ligand-assisted C–H bond activation and arylation of pyridines.[43]

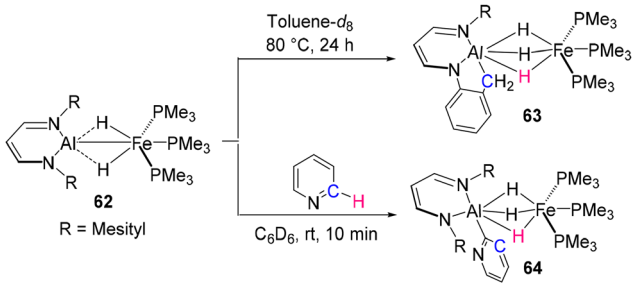

Scheme 25 Cooperative C(sp^2)–H bond activation by an Fe–Al complex.[39]

Crimmin and co-workers reported the synthesis of a low-spin d^6 iron dihydride complex (**62**) featuring an aluminium-based ligand that interacts directly with the hydride ligands (Scheme 25).[39] Upon heating, complex **62** undergoes cooperative intermolecular C(sp^3)–H bond activation to afford complex **63**. Complex **62** was also competent in intermolecular C(sp^2)–H bond activation. The reaction of **62** with pyridine proceeds rapidly and results in highly selective *ortho*-C–H activation of the heteroarene (**64**). Computational studies indicate that, in the case of C(sp^3)–H activation, initial deprotonation by the Lewis basic iron center was followed by coordination of the Lewis acidic aluminium center to the resulting deprotonated CH_2 fragment, leading to the formation of **63**. In contrast, for pyridine activation, deprotonation at the iron centre was again the first step, after which aluminium initially coordinated to the pyridine nitrogen atom. A subsequent, energetically favourable rearrangement involving migration from an Al–N to an Al–C interaction was crucial for the formation of complex **64**.

Conclusions and outlook

As evident from this Frontier article, metal–ligand cooperation (MLC) has emerged as a powerful strategy for facile E–H (E =

B, Si, C, Al) bond activation. The effectiveness of hemilabile ligands in MLC arises not only from their ability to promote heterolytic E–H bond cleavage, but also from the enhanced catalytic efficiency and product selectivity they provide. Fine-tuning the properties of hemilabile ligands, together with appropriate metal selection guided by the HSAB principle, is therefore crucial. Following heterolytic cleavage, insertion of E–H bonds into metal–ligand frameworks *via* MLC gives rise to a wide range of structurally intriguing σ-complexes featuring M–H–E three-centre-two-electron bonds, which have made significant contributions to synthetic chemistry. Although hemilabile ligand-assisted MLC in E–H (E = B, Si, and C) bond activation has grown substantially over the past few decades, main-group element-hemilabile ligand cooperation in bond activation and catalysis remains relatively underexplored.[44] We sincerely hope that future developments in this area will lead to major advances in the field.

Author contributions

The manuscript was written with contributions from all the authors. All authors have given their approval to the final version of the manuscript.

Conflicts of interest

There are no conflicts to declare.

Data availability

No primary research results, software or code have been included, and no new data were generated or analysed as part of this Frontier article.

Acknowledgements

We acknowledge support from the Anusandhan National Research Foundation (ANRF), New Delhi, India, Grant No. CRG/2023/000189. S. S. thanks DST-INSPIRE for the research fellowship. S. M. thanks IIT Madras for the research fellowship.

References

1 (*a*) R. H. Crabtree, in *The Organometallic Chemistry of the Transition Metals*, Wiley-Interscience, New York, 6th edn, 2014; (*b*) K. Saha, D. K. Roy, R. D. Dewhurst, S. Ghosh and H. Braunschweig, *Acc. Chem. Res.*, 2021, **54**, 1260–1273; (*c*) J. H. Docherty, T. M. Lister, G. McArthur, M. T. Findlay, P. Domingo-Legarda, J. Kenyon, S. Choudhary and I. Larrosa, *Chem. Rev.*, 2023, **123**, 7692–7760; (*d*) G. I. Nikonov, Si-H Bond Activation by Transition-Metal Lewis Acids, in *Organosilicon Chemistry: Novel Approaches and Reactions*, ed. T. Hiyama and M. Oestreich, Wiley-VCH, Weinheim, 2019, pp. 87–113; (*e*) Z. Huang, S. Wang, R. D. Dewhurst, N. V. Ignat'ev, M. Finze and H. Braunschweig, *Angew. Chem., Int. Ed.*, 2020, **59**, 8800–8816.

2 (*a*) J. R. Khusnutdinova and D. Milstein, Metal-Ligand Cooperation, *Angew. Chem., Int. Ed.*, 2015, **54**, 12236–12273; (*b*) T. Higashi, S. Kusumoto and K. Nozaki, *Chem. Rev.*, 2019, **119**, 10393–10402; (*c*) L. Omann, C. D. F. Königs, H. F. Klare and M. Oestreich, *Acc. Chem. Res.*, 2017, **50**, 1258–1269.

3 M. D. Wodrich and X. Hu, *Nat. Rev. Chem.*, 2017, **2**, 1–7.

4 I. Moritani and Y. Fujiwara, *Tetrahedron Lett.*, 1967, **8**, 1119–1122.

5 F. Forster, T. T. Metsänen, E. Irran, P. Hrobárik and M. Oestreich, *J. Am. Chem. Soc.*, 2017, **139**, 16334–16342.

6 (*a*) M. R. Elsby and R. T. Baker, *Chem. Soc. Rev.*, 2020, **49**, 8933–8987; (*b*) C. Gunanathan and D. Milstein, *Acc. Chem. Res.*, 2011, **44**, 588–602.

7 (*a*) M. L. H. Green, *J. Organomet. Chem.*, 1995, **500**, 127–148; (*b*) M. L. H. Green and G. Parkin, *J. Chem. Educ.*, 2014, **91**, 807–816; (*c*) A. Amgoune and D. Bourissou, *Chem. Commun.*, 2011, **47**, 859–871.

8 R. G. Pearson, *J. Chem. Educ.*, 1968, 581–587.

9 M. W. Drover, J. A. Love and L. L. Schafer, *Chem. Soc. Rev.*, 2017, **46**, 2913–2940.

10 (*a*) K. Saha, R. Ramalakshmi, S. Gomosta, K. Pathak, V. Dorcet, T. Roisnel, J.-F. Halet and S. Ghosh, *Chem. – Eur. J.*, 2017, **23**, 9812–9820; (*b*) U. Kaur, K. Saha, S. Gayen and S. Ghosh, *Coord. Chem. Rev.*, 2021, **446**, 214106; (*c*) D. K. Roy, B. Mondal, R. S. Anju and S. Ghosh, *Chem. – Eur. J.*, 2015, **21**, 3640–3648; (*d*) R. Borthakur, K. Saha, S. Kar and S. Ghosh, *Coord. Chem. Rev.*, 2019, **399**, 213021; (*e*) S. K. Bose, D. K. Roy, P. Shankahari, K. Yuvaraj, B. Mondal, A. Sikder and S. Ghosh, *Chem. – Eur. J.*, 2013, **19**, 2337–2343; (*f*) R. S. Anju, D. K. Roy, K. Geetharani, B. Mondal, B. Varghese and S. Ghosh, *Dalton Trans.*, 2013, **42**, 12828–12831; (*g*) K. Yuvaraj, D. K. Roy, K. Geetharani, B. Mondal, V. P. Anju, P. Shankhari, V. Ramkumar and S. Ghosh, *Organometallics*, 2013, **32**, 2705–2712.

11 S.-F. Hou, J.-Y. Chen, M. Xue, M. Jia, X. Zhai, R.-Z. Liao, C.-H. Tung and W. Wang, *ACS Catal.*, 2020, **10**, 380–390.

12 (*a*) S. Saha, A. Haridas, F. Assanar, C. Bansal, P. K. S. Antharjanam and S. Ghosh, *Dalton Trans.*, 2022, **51**, 4806–4813; (*b*) S. Saha, S. Mohapatra, M. Kumar, D. Yadav and S. Ghosh, *Inorg. Chem.*, 2025, **64**, 2618–2629.

13 C. Erken, A. Kaithal, S. Sen, T. Weyhermüller, M. Hölscher, C. Werlé and W. Leitner, Manganese-catalyzed hydroboration of carbon dioxide and other challenging carbonyl groups, *Nat. Commun.*, 2018, **9**, 4521.

14 T. Stahl, K. Mether, Y. Ohki, K. Tatsumi and M. Oestreich, *J. Am. Chem. Soc.*, 2013, **135**, 10978–10981.

15 C. C. Comanescua and V. M. Iluc, *Chem. Commun.*, 2016, **52**, 9048–9051.

16 (*a*) K.-S. Feichtner and V. H. Gessner, *Chem. Commun.*, 2018, **54**, 6540–6553; (*b*) L. T. Scharf, J. Weismann,

K. S. Feichtner, F. Lindl and V. H. Gessner, *Chem. – Eur. J.*, 2018, **24**, 3439–3443.
17 M. A. Rankin, K. D. Hesp, G. Schatte, R. McDonald and M. Stradiotto, *Dalton Trans.*, 2009, 4756–4765.
18 M. Zafar, A. Ahmad, S. Saha, R. Ramalakshmi, T. Roisnel and S. Ghosh, *Chem. Sci.*, 2022, **13**, 8567–8575.
19 (*a*) M. Zafar, R. Ramalakshmi, K. Pathak, A. Ahmad, T. Roisnel and S. Ghosh, *Chem. – Eur. J.*, 2019, **25**, 13537–13546; (*b*) A. Ahmad, S. Saha, M. Zafar, T. Roisnel, P. Ghosh and S. Ghosh, *Eur. J. Org. Chem.*, 2023, e202201283; (*c*) S. Gayen, F. Assanar, S. Shyamal, D. P. Dorairaj and S. Ghosh, *Chem. Sci.*, 2024, **15**, 15913–15924.
20 U. Kaur, S. Gayen, H. Sharma, K. Vanka and S. Ghosh, *Chem. – Eur. J.*, 2025, **31**, e202404469.
21 K. D. Spielvogel, J. A. Luna, S. M. Loria, L. P. Weisburn, N. C. Stumme, M. R. Ringenberg, G. Durgaprasad, J. M. Keith, S. K. Shaw and S. R. Daly, *Inorg. Chem.*, 2020, **59**, 10845–10853.
22 G. P. Hatzis and C. M. Thomas, *Chem. Commun.*, 2020, **56**, 8611–8614.
23 (*a*) S. Takemoto, T. Ito, Y. Yamazaki, M. Tsujita and H. Matsuzaka, *J. Organomet. Chem.*, 2016, **812**, 158–166; (*b*) H. Song, K. Ye, P. Geng, X. Han, R. Liao, C.-H. Tung and W. Wang, *ACS Catal.*, 2017, **7**, 7709–7717.
24 M. W. Drover, L. L. Schafer and J. A. Love, *Angew. Chem., Int. Ed.*, 2016, **55**, 3181–3186.
25 S. Saha, P. Chakrabortty and S. Ghosh, *Chem. – Eur. J.*, 2025, **31**, e02125.
26 (*a*) K. Saha, S. Ghorai, S. Kar, S. Saha, R. Halder, B. Raghavendra, E. D. Jemmis and S. Ghosh, *Angew. Chem., Int. Ed.*, 2019, **58**, 17684–17689; (*b*) S. Bairagi, S. Giri, G. Joshi, E. D. Jemmis and S. Ghosh, *Angew. Chem.*, 2025, **137**, e202417170.
27 Z. Zhao, J. Liu, C. Tung and W. Wang, *Chin. Chem. Lett.*, 2023, **34**, 108293.
28 N. Hariharan and C. Gunanathan, *Org. Lett.*, 2025, **27**, 10348–10353.
29 T. I. Gountchev and T. D. Tilley, *J. Am. Chem. Soc.*, 1997, **119**, 12831–12841.
30 (*a*) Z. K. Sweeney, J. L. Polse, R. G. Bergman and R. A. Andersen, *Organometallics*, 1999, **18**, 5502–5510; (*b*) L. C. Stevenson, S. Mellino, E. Clot and P. Mountford, *J. Am. Chem. Soc.*, 2015, **137**, 10140–10143; (*c*) J. Du, L. Wang, M. Xie and L. Deng, *Angew. Chem., Int. Ed.*, 2015, **54**, 12640–12644; (*d*) C. P. Casey, S. W. Singer, D. R. Powell, R. K. Hayashi and M. Kavana, *J. Am. Chem. Soc.*, 2001, **123**, 1090–1100.
31 J. E. Stevens, C. E. Moore and C. M. Thomas, *J. Am. Chem. Soc.*, 2023, **145**, 794–799.
32 W.-Y. Chu, X. Zhou and T. B. Rauchfuss, *Organometallics*, 2015, **34**, 1619–1626.
33 M. Zafar, R. Ramalakshmi, A. Ahmad, P. K. S. Antharjanam, S. Bontemps, S. Sabo-Etienne and S. Ghosh, *Inorg. Chem.*, 2021, **60**, 1183–1194.
34 D. G. A. Verhoeven, A. F. Orsino, R. L. M. Bienenmann, M. Lutz and M.-E. Moret, *Organometallics*, 2020, **39**, 623–629.
35 T. Chu, I. Korobkov and G. I. Nikonov, *J. Am. Chem. Soc.*, 2014, **136**, 9195–9202.
36 J. A. B. Abdalla, I. M. Riddlestone, J. Turner, P. A. Kaufman, R. Tirfoin, N. Phillips and S. Aldridge, *Chem. – Eur. J.*, 2014, **20**, 17624–17634.
37 (*a*) T. N. Hooper, S. Lau, W. Chen, R. K. Brown, M. Garçon, K. Luong, N. S. Barrow, A. S. Tatton, G. A. Sackman, C. Richardson, A. J. P. White, R. I. Cooper, A. J. Edwards, I. J. Casely and M. R. Crimmin, *Chem. Sci.*, 2019, **10**, 8083–8093; (*b*) J. A. Zurakowski, B. Stadler, M. W. Drover and M. R. Crimmin, *Angew. Chem., Int. Ed.*, 2025, **64**, e202512684.
38 P. Zatsepin, T. Moriyama, C. Chen, S. Muratsugu, M. Tada and M. Yamashita, *J. Am. Chem. Soc.*, 2024, **146**, 3492–3497.
39 N. Gorgas, A. J. P. White and M. R. Crimmin, *J. Am. Chem. Soc.*, 2022, **144**, 8770–8777.
40 T. A. Engesser, M. R. Lichtenthaler, M. Schleep and I. Krossing, *Chem. Soc. Rev.*, 2016, **45**, 789–899.
41 M. W. Drover, J. A. Love and L. L. Schafer, *J. Am. Chem. Soc.*, 2016, **138**, 8396–8399.
42 (*a*) M. A. Esteruelas, J. Herrero and L. A. Oro, *Organometallics*, 1993, **12**, 2377–2379; (*b*) A. de Aguirre, S. Díez-González, F. Maseras, M. Martín and E. Sola, *Organometallics*, 2018, **37**, 2645–2651.
43 V. Salamanca, A. Toledo and A. C. Albeniz, *J. Am. Chem. Soc.*, 2018, **140**, 17851–17856.
44 L. Greb, F. Ebner, Y. Ginzburg and L. M. Sigmund, *Eur. J. Inorg. Chem.*, 2020, **2020**, 3030–3047.